

Evolving Cellular Neural Networks for the Automated Segmentation of Multiple Sclerosis Lesions

Eleonora Bilotta, Antonio Ceresa, Pietro Pantano, Aldo Quattrone, Andrea Staino and Francesca Stramandinoli

Abstract This chapter presents an innovative approach for the segmentation of brain images that contain multiple sclerosis (MS) white matter lesions. Quantitative research of Magnetic Resonance Images (MRI) aimed at detecting and studying lesion load and tissue volumes, has turned out to be very useful re evaluation of patients and clinical assessment of therapy. Until now, this has been obtained by using manual delineation of MS lesions, which made the analysis a time consuming process. The application, presented in this work, is a genetic algorithm (GA) that evolves a Cellular Neural Network (CNN) for pattern recognition, capable to segment automatically the brain areas affected by lesions in MRI, and also to immediately eliminate the parts of the brain that are not directly connected to the disease (like the skull, the optic nerve, etc.) in the segmentation process. In comparison to manual segmentations, the proposed method shows a very high level of reliability. It must also be reported, that the relative algorithm is more accurate and it adapts to different conditions of the stimulus. Furthermore, it can create 3D images of the brain regions affected by MS, providing new perspectives of the diagnostic analysis of this disease. The work has practical applications in the medical field. Future industrial development of this work could lead to the embodiment of the algorithm directly into the MRI equipment, because the CNN can be implemented in hardware (via discrete off-the-shelf components) or fabricated as a Very Large Scale Integrated (VLSI) chip.

Eleonora Bilotta · Pietro Pantano · Andrea Staino · Francesca Stramandinoli,
Evolutionary Systems Group, University of Calabria, 87036, Arcavacata di Rende, Italy, e-mail: fbilotta,piepa}@unical.it, {andreasstaino,francescastramandinoli}@gmail.com

Antonio Ceresa · Aldo Quattrone,
Neuroimaging Research Unit, Institute of Neurological Sciences, National Research Council, 88100 Catanzaro, Italy, e-mail: {a.ceresa,a.quattrone}@cisl.cnr.it

1 Introduction

The introduction into the neuroscience field of the functional brain imaging technology has opened the door to new frontiers in the diagnosis of brain diseases. But it has also created a major problem affecting the medical diagnosis, which consists of distinguish, identify and recognize the salient parts of the information produced by the technology, within a very large amount of available data. Indeed, one of the most important problems in medicine is to carry out an accurate diagnosis, just based on this huge amount of data. Human beings make mistakes because of their limited cognitive capacity in managing all this information. Furthermore, a significant drawback is subjectivity in medical diagnosis. Often, the physicians don't use objective criteria in extracting salient clues from MRI, but simply their experience closely related to other, previously made, diagnoses. This means that the diagnostic results do not depend on quantitative data in a clear systematized diagnostic picture, but rely merely on the interpretation of signals from the patient, correlated with data from the MRI [1]. Usually, Artificial Neural Networks (ANNs) are a very effective tool in medical diagnosis and in predicting of clinical outcomes. As well as in other important fields of research such as in business, finance, artificial intelligence, mathematics, cognitive modelling, evolutionary robotics, etc., the most important strong points of ANNs are:

1. they can be trained on examples instead of rules;
2. they do not have the human limitations;
3. they can identify the problem quickly;
4. they can achieve a real-time analysis and make the specific performance related to the application field.

Until recently, the ANNs represented a suitable system for the recognition of brain damage in neurodegenerative diseases [2, 3] and for the management of huge amount of data coming from MRI [4, 5, 6]. Currently, this paradigm has been proved to be ineffective in managing and processing of information on a wide scale [7], that's why other paradigms are taking the place of the ANNs. In particular, for the exceptional quality of their performance, as well as of their ability to process in parallel, in order to ease the use and implementation in both hardware and software, cellular neural networks [8, 9, 10] start to become a dominant model in the field of neuroscience [7, 11, 12, 13]. The CNN "is a large-scale non linear analog circuit which processes signals in real time. Like Cellular Automata (CA), it is made of a massive aggregate of regularly spaced circuit clones, called cells, which communicate with each other directly only through their nearest neighbors. Each cell is made of a linear capacitor, a nonlinear voltage-controlled current source, and a few resistive linear circuit elements" [8]. In comparison with other kind of neural networks, this system has the advantage of being easily implemented in a silicon chip. The dynamics of CNN is always governed by a set of Ordinary Differential Equations (ODEs), which is as large as the number of cells in the

system. The important characteristic of the CNN is to be a meta-model for other systems, both discrete as CA [14] and continuous [15, 16]. The system is particularly suitable for image processing tasks. The later evolution of this system, which is the CNN Universal Machine, is a powerful computer built on a chip. The system has a compiler, an operating system, and a programming system, based on C language, that enables to implement any kind of algorithm for image processing. The sequence of algorithms for image processing is incorporated into the chip, which has the same functions as a digital computer. The CNN paradigm is achieving more and more importance in image processing applications; in fact, a great number of algorithms, based on cellular neural networks, can be found in literature and used for the treatment of images in the most different disciplines. In this chapter, our focus is to use the CNNs in the field of medical diagnosis, where very encouraging and satisfactory results have been obtained. Medical images segmentation and signal processing establish one of the most important area of medical diagnosis, supported by successfully applied CNNs [17]. This diagnosis has magnetic resonance imaging [7, 13], computed tomography (CT) [18, 19] and Electro Encephalo Gramme (EEG) [11]. A CNN based approach to classify MRI with respect to the presence of mesial temporal sclerosis has been presented by Döhler et al. in 2008 [7]. Multiple sclerosis is a demyelinising disease of the central nervous system that leads to inflammatory pathology. MS pathology is primarily expressed as focal lesions in the white matter of the brain. Because of its superior contrast, MRI serves as the modality of choice for clinical evaluation of MS. Generally, manual delineation of MS lesions is time-consuming, because three-dimensional information from several magnetic resonance contrasts must be integrated. In the last years, there has been increasing interest in developing novel techniques for automated MS lesions segmentation. In this paper we present an automated approach to segment MS lesions in MRI. Through the evolution of CNN, based on genetic algorithms, we have developed a system that precisely identifies demyelinated brain areas, due to the neurodegenerative disease. This approach has been tested on a data set of 11 patients, who underwent structural MRI and who have been diagnosed with MS. For each patient, 24 slices were analysed, which cover the whole brain. The results show a very high percentage of agreement (almost 80%) with manual segmentation. The exposed method has given satisfactory results, showing that, after the learning process, the CNN is capable to detect MS lesions with different shapes and intensities. The technique we propose is a fully automatic method and does not require manually segmented data.

This work is organized as follows. After the introduction, the second section clearly identifies the problem that the chapter intends to address and solve. It also presents the most relevant aspects of this research field and their implications for the future development of this sector. Related works, item-

izing the most important issues and concerning both the medical diagnosis and the use of CNN in the neuroscience discipline, are presented in the third section. The fourth section clearly identifies the approach we have used. This section presents the mathematical aspects of both CNN and GA models, the optimization approach we have implemented and the integration in the real life context of medical diagnosis. The fifth section presents the experimental results on the performance measurements, the statistical evaluation of the results and the comparison with manual segmentation. Conclusions and future work, contained in section seventh and eighth respectively, close this chapter.

2 The Automatic segmentation of Multiple Sclerosis by using a CNN

Multiple sclerosis is a debilitating and progressive autoimmune disease that causes inflammation, demyelination, and axonal damage of the Central Nervous System (CNS) [20, 21, 22]. Used in most clinical trials, the Expanded Disability Status Scale (EDSS) is a method to analyze functional damage to motor, cognitive and sensory systems [23] in people with MS damages. This method not only provides a quantification of disability, but also serves to monitor changes in the level of disability over time. Devised by John Kurtzke in 1983 [24] and following his previous assessment system (Disability Status Scale, or DSS), the EDSS ranges from 0 to 10, with increments of 0.5 units. The score is based on an examination done by a neurologist and based mainly on the impairment of motor activity. EDSS steps 1.0 – 4.5 identify people who are able to walk without help, even if they have MS. EDSS steps 5.0 – 9.5 categorize the complete impairment of motor activity. The method also recognizes eight functional systems (FS) that may be affected, which can produce a huge amount of symptoms, from the speech to the sensory modality impairments, without any patterns. Each functional system is scored on a scale from 0 (no disability) to 5 or 6 (severe disability). Regarding the cognitive disability, the Paced Auditory Serial Addition Test (PASAT) [25] is a frequently used test for capturing deficits of attention and working memory in MS subjects. The assessment of onset and progression of MS diseases is critically dependent on identification of lesions or changes in white matter regions of the brain, through many techniques of brain imaging, and especially through MRI. The most important problems that researchers encounter in this domain are the following:

1. the inhomogeneous, dramatically complex structure of the brain [26];
2. the unpredictability of the disease that affects different areas of the brain and other nervous structures, without a defined pattern;
3. the lack of clear correlation between the amount of damaged brain areas and the related clinical symptoms [27];

4. the lack of highly defined technical standards in brain imaging processing, that introduces in MS lesions segmentation methods a wide range of technological bias [28].

Many mathematical models have been used to develop methods for brain MRI segmentation [29, 30]. They are concerned to discriminate lesions for different diseases [31, 32, 33], to identify changes in anatomical structures [34], and also to create hardware and software applications for 3D brain visualization. The process of image segmentation precisely allows to achieve this analysis both for training the neurologists and for research purposes (The Whole Brain Atlas, <http://www.med.harvard.edu/AANLIB/home.html>). As Filippi et al. [35] pointed out, MS diagnosis can be done by analyzing T2-weighted images, while for monitoring the evolution of the disease, it is necessary to obtain efficient measures of the Total Lesion Load (TLL), by using lesion segmentation techniques based on signal intensity thresholds. To analyze these problems, Souplet et al. [36] present a comprehensive *state of the art* classification of the most representative systems for MS lesions segmentation. Shiee et al. [37] use a segmentation method based on topological and statistical atlases, while all the segmented structures are topologically constrained, allowing a further segmentation of shapes. In the literature on these topics, it is noted that the processes of segmentation usually require a trade-off between accuracy and computation time. Due to these problems, many segmentation algorithms, based on artificial neural networks, have failed to give satisfactory results [7]. ANNs, developed in the last decades, are connectionist systems that simulate the biological mechanisms of information processing. They have been widely used in medical science and biomedical research, especially as pattern recognition systems, as medical expert systems to make predictions, as systems to monitor the status of some diseases such as cancer and as MRI segmentation systems. Recently, ANNs with many layers have been established [38], and usable algorithms have been implemented. Although the ANNs, one of the leading paradigms of machine learning during the 1980's [39], have been dropped in favor of simpler methods of classification to define and manage the task of recognition / segmentation / forecast, more efficient methods from the computational point of view, achieving superior performance compared to ANN approaches, have been implemented. The main reason lies in the fact that the algorithm of back propagation is not practical for training a network that has more than two or three layers, and the computational load of multi-layers ANN architectures is very high. Cellular neural networks allow to solve, or at least, to mitigate, those problems; they can be regarded as one of the paradigms of the Science of Chaos and Complexity. CNNs are massively parallel systems, easily integrated in silicon, and mainly used for advanced image recognition, especially in medical and graphic fields.

In this chapter, we describe a new application based on genetic algorithms that evolves a cellular neural network capable to automatically determine the TLL in multiple sclerosis patients. Our study aims to analyze MRI and to obtain reliable and reproducible measures of the total lesion load in patients with MS. The process of segmentation, that we have developed, is based on adaptive approaches. These approaches can be applied to different clinical settings, having as output different types of images. It must be noted that CNNs are chaotic non linear systems. The introduction of nonlinear dynamics in the field of brain imaging will lead to the acquisition of already well established methods and concepts [40]. Many important outcomes can be applied because the methods, concepts and visualization systems, already developed in the field of nonlinear dynamic systems [41, 42, 43, 44, 45, 46], can improve the segmentation of MRI, the study of brain shapes and their evolution and the 3D display of the brain, revisiting by the chaos theory the dynamics and the patterns with which the neurodegenerative diseases occur. The future implications of those new methods and concepts in the field of brain imaging are promising, because they would re-examine the traditional approach through completely automatic and very reliable methods from the computational point of view, both in terms of consistency of the systems' performance and in checking of the disease evolution. Scientific potentials in the intersection of Chaos and Complexity Theories and the brain imaging technologies are fully to be explored and exploited for the future development of this sector.

3 Related Works

3.1 Related Work in the Problem Domain

In these last decades, the rapid collection of brain images of healthy and unhealthy people has inspired the development of mathematical algorithms, that compare sets of brain data in a huge number of subjects all over the world. New methods of machine vision [47, 48, 49, 50, 51], new interface [52], the construction of the anatomical model [53], the use of differential geometry [54, 55] were developed to represent the great variations in the brain, and to identify disease specific models [56]. These models can also identify qualitative and quantitative patterns of their anatomy in relation to their function [57], highlighting the surprising relationships between genotype and phenotype.

As we have already said in the previous sections, MS pathology presents focal lesions in the white matter of the brain. For its particular properties of providing much greater contrast for the different soft tissues of the body, magnetic resonance is the technology used for clinical evaluation of MS. The delineation of the disease is handmade by experienced neurologists. It varies

from person to person and it is a very labor-intensive and time-consuming task. Many mathematical models have been used to implement automated MS lesion segmentation algorithms and systems. There are many segmentation methods, the automated methods and the Atlas-based segmentation methods. Among the automated methods, there are also several classes. The first one classifies the lesions as outliers of the normal brain tissues, together with a system for the delineation of the lesion borders [58, 59, 60, 61, 62]. Contrariwise, the second class of methods instead shapes the lesions as a separate set [63]. All these methods try to establish an increasingly precise delineation to make the process of identification of MS lesions accurate and to define the total MS lesion load. These techniques have many problems [37]. Several of these methods are only based on the lesions segmentation process, ignoring the quantification of the volume of the brain injured area [64]. These methods also do not pay attention to the sub-cortical structures of the brain, to the cortical surface analysis and they do not consider the degree and the location of brain atrophy, which is a crucial variable for evaluating the evolution of MS. None of these methods consider the special topology of patients with MS, altered by the lesions. Furthermore, in order to define the outliers, many algorithms are heavily dependent on the threshold choice, and often the process is not completely automated.

3.2 Related Work in the Optimization Domain

The domain of optimization of this chapter relates to processes for automatic segmentation of MRI. As we said earlier, the mapping of the brain covers often hundreds or even thousands of images [65, 66, 67]. To address these problems in terms of processing speed, computational effectiveness, automated image registration and warping methods, many algorithms must filter the information from these images automatically [68]. For fast image segmentation and labeling, there were also developed other techniques and even modern technology of 'IC was used in this field. Databases with topics related to active brain are active and they increase worldwide at a almost exponentially rate ([http://www.sfn.org/index.aspx?pagename=NDG_main;
http://brancusi.usc.edu/bkms/](http://www.sfn.org/index.aspx?pagename=NDG_main;http://brancusi.usc.edu/bkms/)). A huge community of researchers analyze brain images through client-server software technologies. These intensive analysis can be performed on a remote server, with the help of supercomputing resources, aimed to discover many general trends for many degenerative diseases [69]. These advances in technology and infrastructure have enabled the creation of a population-based atlas of the brain [70]. These atlases combine imaging data from healthy and diseased populations and are leading to the creation of communities of users in the field of neuroscience. The atlases are an important source of information for scientists as they describe how the brain varies with age, sex and demographics. They also provide a comprehen-

sive approach to the study of a particular subgroup of the population, with a specific disease or a specific disorder, such as that discussed in this chapter on multiple sclerosis. Generally in the MRI segmentation domain, supervised segmentation algorithms normally work according to one of two paradigms for guiding the automatic or semiautomatic process. The steps are as follows:

1. Specification of sections of the borders of the chosen object or of a closed complete border that develops to the chosen border;
2. Specification of a small set of pixels, belonging to the chosen object and to a set of pixels, belonging to the background.

Furthermore, any of the automatic segmentation algorithms might be considered supervised by following expert clinicians selection of the desired segment. However, if the desired object is not an entire segment, another clustering/segmentation algorithm must be used to divide or combine the automatic segments. In fact, while semiautomatic methods are highly dependent on the choice of an appropriate threshold (to effectively detect lesions) and on the experts selection of the desired target brain areas, our algorithm, improving the method already developed by Döhler [7], allows for obtaining the desired output by programming a fully automated strategy on the entire data set, without the need of external calibration. The images, acquired by the magnetic resonance scanning, have, from patient to patient, sometimes significant differences in the intensity of grey and in the area of the injuries. Differences can be observed also from a slice to another one. For this reason, it is necessary to train the CNN to become adapted to different input conditions, not encountered before. By evolving the CNN templates, we have been able to determine most of the lesions in all the patients, optimizing the present problem. The system could provide a useful support tool for the evaluation of lesions in MS, and particularly to assess the evolution of the lesions. It is worth noting that our analysis was carried out on two-dimensional slices. Another improvement, about what was already reported in the work of Döhler et al. [7], is the possibility to extend our results by working on volumes of data, rather than processing planar images. 3D CNNs [71] may represent a new and powerful tool for the development of applications for supporting of medical diagnosis. By exploiting information provided by a three dimensional representation of the brain, the evolution of the 3D network can lead to a significant improvement of the performances. For this reason, by modifying the architecture of the standard CNN, we propose a 3D CNN model that is able to handle and perform different functions on objects in a three dimensional space. An innovative library of 3D templates has been implemented, that allows the execution of interesting and efficient operations. We used genetic algorithms for 3D template learning; this means that even a 3D CNN can be trained by a learning algorithm in such a way that, during the training process, the network learns the configuration for performing the desired operation.

4 The Approach

The approach, adopted in this work, is based on genetic algorithms and cellular neural networks, that represent the mathematical tools that we have used to tackle the problem of automatically detecting MS lesions in MRI, which presence is revealed by regions in the brain that are brighter than their surroundings (Figure 1).

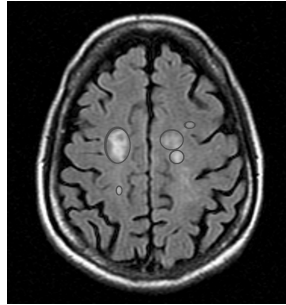


Fig. 1: MS lesions in the white matter of the brain. Lesions are brighter than other tissues in MRI.

In what follows, we give a short description of the CNN paradigm and we present the key features of genetic algorithms. Cellular neural networks [8] are an array of nonlinear programmable analog processors, called cells, that perform parallel computation. The key idea behind the CNN paradigm was that to combine the main advantages of cellular automata and artificial neural networks [8]. Like neural networks, a CNN is a nonlinear analog circuit which is capable of processing a large amount of data in real time and in an asynchronous way. At the same time, the structure of cellular neural networks is similar to that found in cellular automata, because interactions between cells are only local, that is each cell is physically connected only with its nearest neighbours. From a mathematical point of view, each cell is a dynamical system whose state evolves in time, according to a specific mathematical model, and whose output is a nonlinear function of the state. For the image processing purpose, the most usual architecture is a regular two dimensional grid, in which each processing unit directly interacts only with the neighbouring cells, located within a prescribed sphere of influence; given a CNN of $M \times N$ cells, the neighbourhood $S_{ij}(r)$ of radius $r \geq 0$ for the cell C_{ij} is the set of cells, satisfying the following property:

$$S_{ij}(r) = \{C_{kl} : \max(|k - i|, |l - j|) \leq r\}, \quad 1 \leq k \leq M, 1 \leq l \leq N \quad (1)$$

The grey box in Figure 2 highlights the sphere of influence $S_{ij}(1)$ of the cell at position (i, j) , whose neighbourhood comprises nine elements (the eight adjacent units and the cell itself).

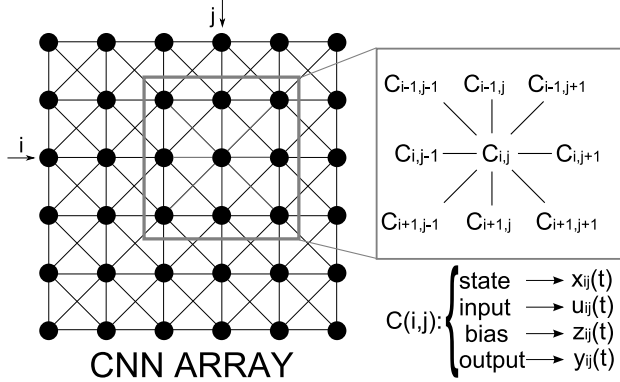


Fig. 2: A cellular array whose elements represent nonlinear dynamic systems.

A sphere of influence of radius $r = 1$ corresponds to a 3×3 neighbourhood, one of radius $r = 2$ to a 5×5 neighbourhood and so on. Referring to the central grey unit, neighbourhood of different sizes are shown (Figure 3).

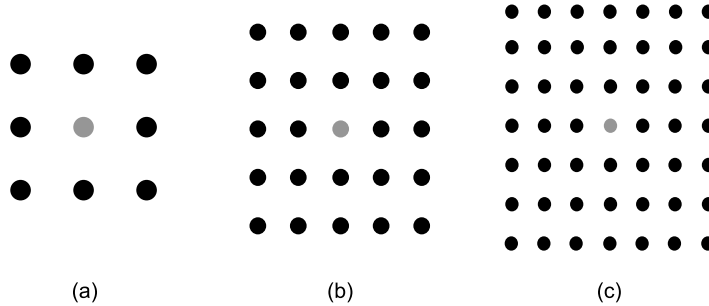


Fig. 3: Neighbourhood of radius $r=1$ (a), $r=2$ (b) $r=3$ (c) for the considered grey unit.

Each cell C_{ij} is characterized by four time variables, called the *state* $x_{ij}(t) \in \mathbb{R}^n$, that generally is not observable from the outside, the *input* $u_{ij}(t) \in \mathbb{R}^u$, corresponding to external stimuli provided to the cell, the *output* $y_{ij}(t) \in \mathbb{R}^p$, that represents the value that can be observed and measured, and an additional input $z_{ij}(t) \in \mathbb{R}^z$ called *bias*. The dynamics of a $M \times N$ CNN is described by $M \times N$ coupled differential equations (2), modelling

the evolution of the state of each cell and its interaction with its neighbors (“coupling laws”).

$$\begin{aligned} \dot{x}_{ij}(t) &= g(x_{ij}(t), z_{ij}(t), \underline{u}_{kl}(t), f(\underline{x}_{kl}(t))), \quad (k, l) \in S_{ij}(r), \\ i &= 1 \dots M, j = 1 \dots N \end{aligned} \quad (2)$$

where $\underline{u}_{kl}(t)$ e $f(\underline{x}_{kl}(t))$ denote vectors, whose components are the input and the output of the neighbors of C_{ij} . The output of each cell is obtained by applying the nonlinear algebraic function $f(x_{ij}(t))$, such that:

$$y_{ij}(t) = f(x_{ij}(t)) \quad (3)$$

Standard nonlinearity for the output equation is given by the following expression:

$$y_{ij}(t) = f(x_{ij}(t)) = \frac{1}{2} [|x_{ij}(t) + 1|] - [|x_{ij}(t) - 1|] \quad (4)$$

which characteristic is shown in Figure 4.

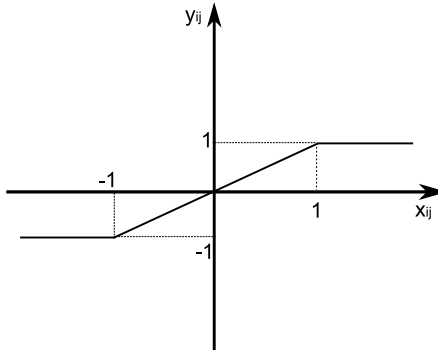


Fig. 4: Standard nonlinearity for the output equation.

It is worth noting that (1) is not completely defined for cells lying on the boundaries of the array, whose sphere of influence extends beyond the boundary of the given CNN. Therefore, it is necessary to introduce some additional elements to the array, called virtual cells, whose state and input are given in accordance with the boundary conditions of the network. The following types of boundary conditions are proposed:

1. Fixed (or Dirichlet): values of the *virtual cells* are given as a prescribed constants;
2. Zero-flux (or Neumann): values of the *virtual cells* are the same as the corresponding *boundary cells*;

3. Periodic (or toroidal): values of the virtual cells are the same as the boundary cells on the opposite side (e.g., top *virtual cells* have the value of bottom *boundary cells*).

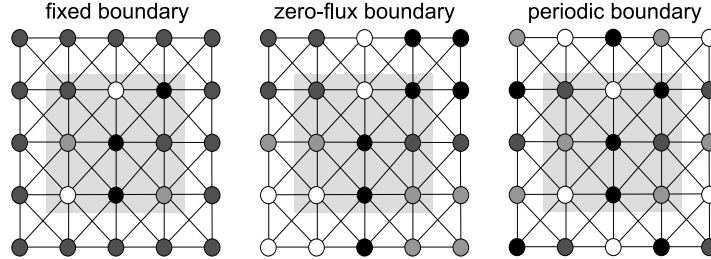


Fig. 5: Boundary conditions commonly used for CNNs.

Different kinds of boundary conditions for a 3×3 CNN (whose cells belong to the shaded grey area) are shown in Figure 5; the values for the virtual cells are set according to the corresponding chosen boundary conditions. By choosing an appropriate g function in (2), different models of cellular neural networks can be defined. In this work, we will deal with the **standard CNN model**, in which each cell C_{ij} is a first order dynamical system, i.e. its state is a scalar quantity ($x_{ij}(t) \in \mathbb{R}$) that can be associated with the intensity of a physical variable at the corresponding point in space at time t . For ease of notation, we will omit the time argument of the variables associated to C_{ij} . The set of ODEs that describes the dynamics of a standard CNN is:

$$\frac{dx_{ij}}{dt} = -x_{ij} + \sum_{C(k,l) \in S_r(i,j)} A(i, j; k, l; t) y_{kl} + \sum_{C(k,l) \in S_r(i,j)} B(i, j; k, l; t) u_{kl} + z_{ij} \quad (5)$$

where $A(i, j; k, l; t)$ and $B(i, j; k, l; t)$ represent respectively the weights by which outputs and inputs of the cells in the neighbourhood contribute to changes in the state of C_{ij} . The feedback coupling parameters $A(i, j; k, l, t)$ and input coupling parameters $B(i, j; k, l, t)$ can be used to change and control the strength of interactions between cells and, in general, can vary both in space and time. Being given input, initial state and boundary conditions for each cell C_{ij} such that $1 \leq i \leq M$, $1 \leq j \leq N$, the dynamics of a two-dimensional standard CNN are uniquely specified by the synaptic weights between a cell and its neighbors. These parameters, together with the bias $z_{ij}(t)$, define a CNN template that can be expressed in the form $\{A(i, j; k, l, t), B(i, j; k, l, t), z_{ij}(t)\}$. The operation performed by a cellular neural network on the input data is fully defined by the set of coefficients in the CNN template. If the pattern of interconnection is the same for each cell and does not vary in time, the weighting coefficients can be arranged in

a feedback matrix $A \in \mathbb{R}^{(2r+1) \times (2r+1)}$, and a feedforward or control matrix $B \in \mathbb{R}^{(2r+1) \times (2r+1)}$, while the bias $z_{ij}(t) = z \in \mathbb{R}$ for each (i, j) and t ; in this case, the template reduces to the triple $\{A, B, z\}$. As we will see, an evolutionary approach can be used in order to find a template that allows to obtain a desired operation. As it was stated in the introduction, the key feature of CNNs is their ease in implementation in VLSI chips; in fact, the main difference between CNN and other neural network paradigms is that in the first case information is directly exchanged just between neighboring units so, when it comes to physical realization, cellular neural networks show more flexibility than ANNs, allowing easier integration in silicon devices and greater efficiency in computation. In the original model [8], each CNN cell is a simple nonlinear analog circuit (Figure 6), composed of a linear capacitor, an independent current source, an independent voltage source, two linear resistors and at most $2m$ linear voltage-controlled current source, m being the number of neighbours cells of the considered unit. The voltage $v_{x_{ij}}(t)$ across the capacitor is the state of the cell C_{ij} , while $v_{u_{ij}}$ and $v_{y_{ij}}(t)$ represent the input and the output respectively.

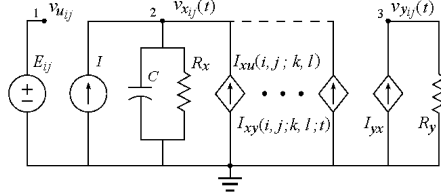


Fig. 6: Original CNN cell model.

The characteristics of the generators $I_{xy}(i, j; k, l; t)$ and $I_{xu}(i, j; k, l)$ are defined as:

$$\begin{aligned} I_{xy}(i, j; k, l; t) &= A(i, j; k, l) v_{y_{kl}}(t) \\ I_{xu}(i, j; k, l) &= B(i, j; k, l) v_{u_{kl}} \end{aligned} \quad (6)$$

The equations (6) state that the current sources $I_{xu}(i, j; k, l)$ are controlled by the input voltage of the neighbors C_{kl} , while the others $I_{xy}(i, j; k, l; t)$ get a feedback from the output voltages of the neighbors cells. In such a way, it is possible to control the strength of interactions between cells by setting the coupling parameters $A(i, j; k, l)$ and $B(i, j; k, l)$. The output $v_{y_{ij}}(t)$ is determined by the nonlinear voltage controlled current source I_{yx} that is the only nonlinear element of the cell and it is characterized by the following equation:

$$I_{yx} = \frac{1}{R_y} f(v_{x_{ij}}(t)) \quad (7)$$

where f is the characteristic function of the nonlinear controlled current source defined as:

$$f(v_{x_{ij}}(t)) = \frac{1}{2}(|v_{x_{ij}}(t) + 1| - |v_{x_{ij}}(t) - 1|) \quad (8)$$

Using the Kirchhoff laws, the state of a CNN cell can be described by the following nonlinear differential equation:

$$C \dot{v}_{x_{ij}}(t) = -\frac{1}{R_x} v_{x_{ij}}(t) + I + \sum_{C_{kl} \in S_{ij}(r)} (A(i, j; k, l)f(v_{x_{kl}}(t)) + B(i, j; k, l)v_{u_{kl}}) \quad (9)$$

that, by considering $1 \leq i \leq M$, $1 \leq j \leq N$, corresponds to the system of ODEs (5). Chua and Roska [10] propose CNNs as a parallel computing paradigm, especially suited for processing analog array signals, with important applications in image processing, pattern recognition, numerical solution of PDEs and investigation of nonlinear phenomena. CNNs have been successfully applied in various image processing applications, especially because of the high pay-off offered by the CNN based architectures [40]. Cellular neural networks can be trained by learning algorithm in such a way that, during the training process, the network learns which is the best configuration for performing a given task. In this work genetic algorithms have been applied in order to evolve a CNN capable of detecting MS lesions from MRI. As is shown in the work of J.H. Holland in 1975 [72], genetic algorithms are computational bio-inspired methods for solving problems; inspired by Darwinian evolution, genetic algorithms are based on the principles of *genetic variation* and *natural selection*. These algorithms simulate the evolution of a population of individuals (Figure 7), which represent possible solutions to a given problem.

Population P of GA												
1	0	1	1	1	0	1				1	0	0
1	1	1	0	1	0	1				1	0	1
1	0	0	1	1	0	1				0	0	0
1	0	1	0	1	0	1				1	1	0

Fig. 7: Population of a genetic algorithm.

To evaluate the performance of each individual in relation to the problem, it is possible to define an appropriate fitness function, which quantitatively measures the performance of each individual, in a given generation and for all the generations. The standard method for developing a GA is to choose a genetic representation, a fitness function and then proceeding with the following steps:

1. Generating a random number of strings (initial population), that encode possible solutions to the problem;
2. Decoding of the genotypes of the population and assessment of each individual (phenotype), according to the fitness function;
3. If the current population contains a satisfactory solution, the algorithm stops.
4. If the system doesn't find a *good* solution, a new evolution starts, generating a new population of individuals, by applying the operators of selection, crossover and mutation.

The process continues with the evaluation of new individuals through the fitness function and continues cyclically in this manner until a satisfactory solution to a given problem is obtained (Figure 8).

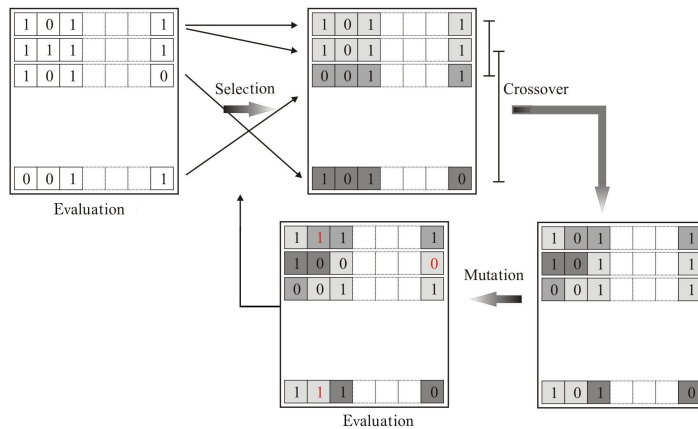


Fig. 8: Steps of a genetic algorithm.

Selection, Crossover and Mutation operators proposed by Holland, are inspired by natural selection and genetics; in particular:

1. **Selection:** it takes place according to a probability that is proportional to the fitness value, in order to give preference to most performant individuals, allowing them to transmit their genes to the next generation.
2. **Crossover:** two individuals are randomly chosen from the population, using the selection operator and new “child” genotypes are created.

3. **Mutation:** once new individuals are generated by crossover operator, some of their genes may undergo mutation process, that means that, according to a given probability, newly created genotypes will have some of their bits flipped.

In image processing applications, a neighborhood of radius $r = 1$ is commonly used and, in most cases, space-invariant templates are chosen, that is the operators $A(i, j; k, l)$ and $B(i, j; k, l)$ depend only on the relative position of a cell with respect to its neighbours. With such assumption, the whole system is characterized by a 3×3 feedback matrix A , a 3×3 control matrix B and a scalar z . Therefore, 19 parameters are needed to “program” a cellular neural network; this means that, once initial state and boundary conditions have been assigned, the operation performed by the CNN on a given input image is determined only by 19 real values that completely define the properties of the network. For our aim, which is to design a genetic algorithm to search for the weights of a standard two-dimensional space invariant CNN, in which each cell has a radius of influence $r = 1$, it is convenient to adopt a representation of templates in vector form. To this purpose, the 19 parameters that define the triple $\{A, B, z\}$ are arranged in an array consisting of 9 feedback synaptic weights defining the A matrix, 9 control synaptic weights defining the B matrix and the threshold z (Figure 9). These 19 coefficients represent a gene for the CNN, associated with a particular function performed by the network.

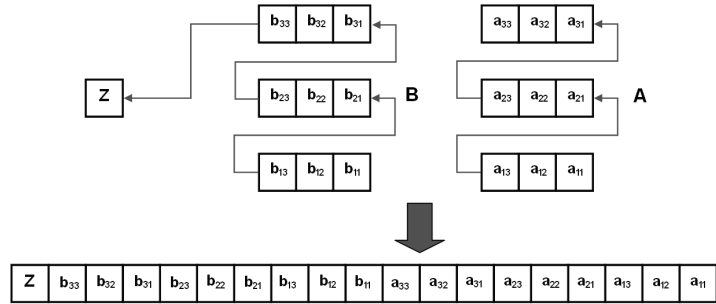


Fig. 9: Representation of a CNN template in vector form.

The genetic algorithm has been designed to get a template to be used for image processing applications. For this reason, we have chosen to impose that the matrices A and B are symmetric with respect to their central element. In this way, we set the conditions for the stability of the CNN, provided in the complete stability theorem [8], which ensures the convergence of the network. It also reduces the computational load of the algorithmic search, since it is necessary to determine only 11 coefficients, 5 belonging to the matrix A , 5

to the matrix B and 1 corresponding to the threshold z . Each genotype is therefore represented by a vector G of 11 elements:

$$G = [a_{11} \ a_{12} \ a_{13} \ a_{21} \ a_{22} \ b_{11} \ b_{12} \ b_{13} \ b_{21} \ b_{22} \ z]. \quad (10)$$

To assess the fitness of a CNN gene compared to an assigned problem, we introduce a target image T of $M \times N$ pixels to be used for training the network. Applying the template corresponding to G and providing an input image to the CNN, it generates as an output an image I^G which can be compared with T , through the cost function:

$$\text{diff}(G) = \sum_{i=1}^M \sum_{j=1}^N I_{ij}^G \oplus T_{ij}. \quad (11)$$

where the operator \oplus denotes the logic xor between the element in position (i, j) of the target image and the corresponding pixel in the CNN output. The fitness function for each phenotype CNN^G , then, is evaluated by calculating the number of equal pixels between T and the CNN output:

$$\text{fitness}(\text{CNN}^G) = M \times N - \text{diff}(G). \quad (12)$$

Hence, the fitness measures the number of equal pixels between the target image and that obtained from the CNN simulation. In this way, higher values of fitness are associated with phenotypes corresponding to templates that produce outputs with a high number of pixels, that coincide with the image target.

4.1 Optimization Approach

A set of evolutionary runs has been performed in order to reach the best level of performance of the developed systems. In our implementation, we have run an initial random population of 35 – 60 individuals, making them evolve for a maximum of 500 generations; “*weighted roulette wheel selector*” and “*best chromosome selector*” were used as selection methods; mutations and elitism strategies were applied. In order to reduce the computational effort due to the large search space, we have chosen to constrain the elements of each genotype to be in the range $[-8, 8]$. The GA was conducted as follows: after evaluating the fitness of each phenotype, the elite individual, i.e. the most performing one, has been directly copied in the next generation; a number of single-point crossover operations, depending on the population size, has been performed. In our experiments, we have used a crossover rate in the range from 30% to 70%. Mutations have been randomly applied in order to prevent trapping into local minima. The elements of the genotypes in the population have been randomly mutated according to a given mutation

rate, each coefficient had a given probability of being changed by a randomly selected real number that falls in the chosen interval $[-8, 8]$. Using a mutation rate of 0.05, each component had 5% probability of being changed, resulting in $\frac{1}{20}$ parameters being mutated on average. Once genetic operators have been applied, a fixed number of genotypes has been selected and moved on the next generation. Obviously, the selection has been guided by the fitness, i.e. higher probabilities of survival have been associated to phenotypes providing higher fitness values. Figures 10-11 show two of the evolutionary runs that we have performed.

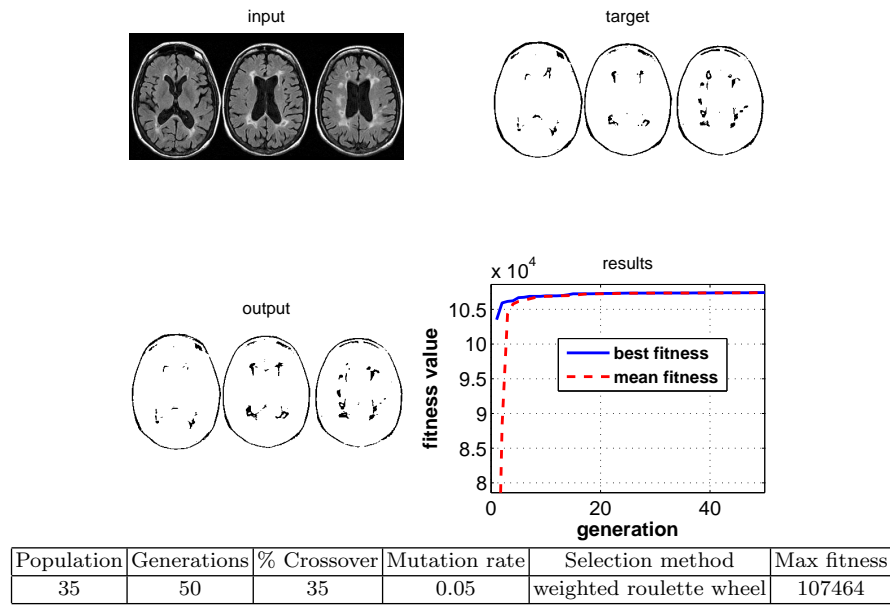


Fig. 10: Results of an evolutionary run that we have performed. The initial population is composed of 35 individuals; the run has evolved 50 generations with a mutation rate of 0.05 and a 35% of crossovers. The *weighted roulette wheel selector* has been the selection method we have used. The highest fitness reached is 107464; by referring that value to the size of the target image, we have obtained an overlapping of 0.9851 with respect to the target (1 being a total agreement).

A number of trials have been performed according to the genetic algorithm scheme described above, some of which are reported in Table 1. In our experiments, the GA achieved a maximum fitness value of 0.9851, resulting in 98.51% of overlapping between the CNN output and the corresponding target image. The average fitness value obtained over the evolutionary runs performed is 0.9820.

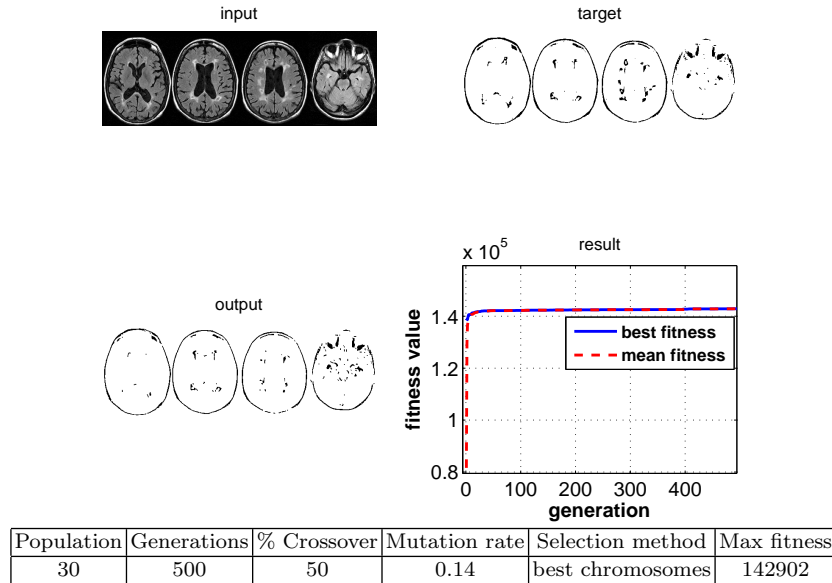


Fig. 11: Evolutionary run we have performed. The initial population is composed of 30 individuals; the run has been evolved for 500 generations with a mutation rate of 7 and a 50% of crossovers. The *best chromosomes selector* has been the selection method we have used. The highest fitness reached is 142902, resulting in 0.9830 of overlapping with the target.

Population	Generations	% Crossover	Mutation rate	Selection method	Max fitness	Normalized fitness
35	50	0.35	20	weighted roulette wheel	107464	0.9851
35	100	0.35	20	weighted roulette wheel	289617	0.9833
30	300	0.3	20	best chromosomes	107392	0.9845
30	500	0.5	7	best chromosomes	142902	0.9830
60	50	0.5	5	best chromosomes	142456	0.9799
40	40	0.7	5	best chromosomes	142697	0.9816

Table 1: Evolutionary runs performed according to the proposed GA based learning process.

At the end of the training process, the following template has been selected:

$$A = \begin{bmatrix} -3.51879 & 3.42019 & -3.48386 \\ 6.47032 & 7.75293 & 6.47032 \\ -3.48386 & 3.42019 & -3.51879 \end{bmatrix} \quad B = \begin{bmatrix} 1.33076 & -3.86887 & 1.53728 \\ -2.30849 & -7.76398 & -2.30849 \\ 1.53728 & -3.86887 & 1.33076 \end{bmatrix} \quad z = -4.81797 \quad (13)$$

Given a MRI slice, by tuning the CNN standard model (5) according to the parameters (13), the system is able to generate images in which MS lesions are isolated from the brain matter, as learnt during training; this is the key-step on which the segmentation algorithm is based.

4.2 Application of the Optimization Approach

One practical application based on the optimization performed by genetic algorithms consists of evolving a CNN capable of supporting neurological diagnosis in order to determine the lesion load in patients affected by multiple sclerosis. To evaluate the evolution of the disease, images acquired by magnetic resonance can be used by neurologists, in order to detect the presence of lesions in the white matter of the brain. The main issue is to develop a CNN algorithm for supporting image analysis and identifying brain areas affected by lesions in MRI. Magnetic resonance scanners acquire gray scale images; each image represents a “slice” corresponding to a volumetric portion of the brain. The main purpose of the algorithm, for each slice, is to generate a binary image as output, in which the lesions are isolated from healthy tissue. In this way, knowing the size of the voxels of the slice, it is possible to calculate an estimate of the lesion load due to the pathology. Although the pixels corresponding to the lesions are always brighter than the others in healthy tissue, they are not the brightest in the image, therefore it is not enough to simply apply a single template that performs a binarization according to a given threshold. CNN, therefore, must be trained to distinguish and classify only the areas actually affected by injuries.

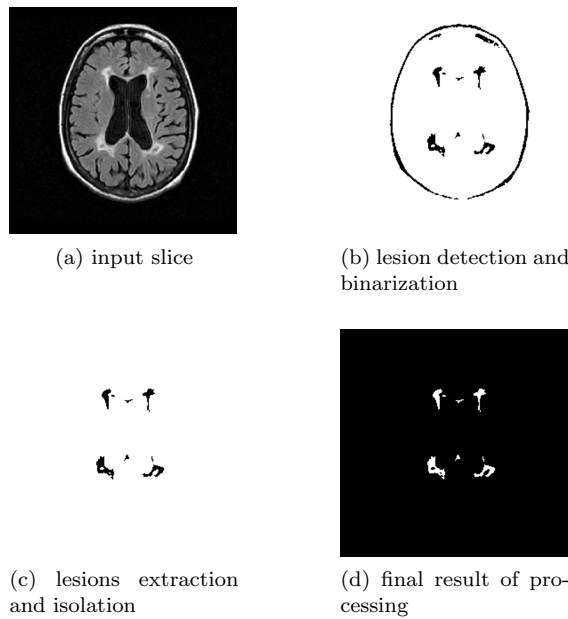
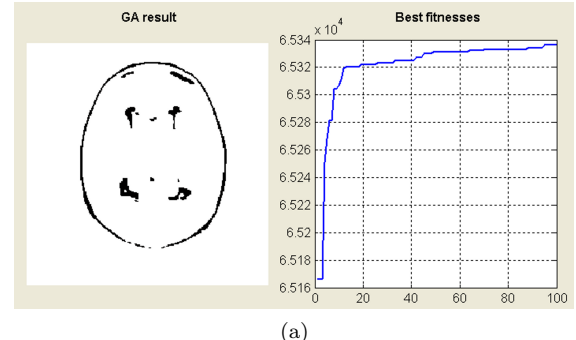


Fig. 12: CNN algorithm for lesions detection in patients affected by MS.

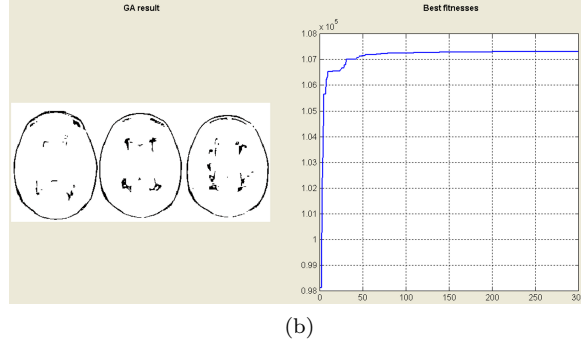
As shown in Figure 12, the algorithm proposed for the segmentation of the MS lesions consists of three principal steps:

1. Lesions detection and their binarization;
2. Segmentation of the white matter of the brain;
3. Lesions extraction and isolation.

The first step of the algorithm has been faced by using genetic algorithms, to determine the weights that allow CNN to generate as output a binary image in which the healthy brain matter is removed. Then, templates in the CNN library [19] were applied for extracting features of interest, eliminating the pixels corresponding to the skull. Since lesions have different shapes and intensity, that vary from slice to slice, even for the same patient, it is necessary to iterate the training process of the network more times, for each iteration providing target images showing different characteristics, so that the CNN can be able to “learn” how to perform the task in a more accurate way (Figure 13).



(a)



(b)

Fig. 13: Training of CNN by GA for the detection of lesions in MRI.

To implement the second step of the algorithm, we have performed a masking operation based on the templates proposed in the library [19] for the

extraction of objects. The idea is to extract from the image obtained in the previous step only objects lying in the slice corresponding to the brain matter; thus at the end of the simulation only lesions will emerge, while areas related to the skull will be deleted.

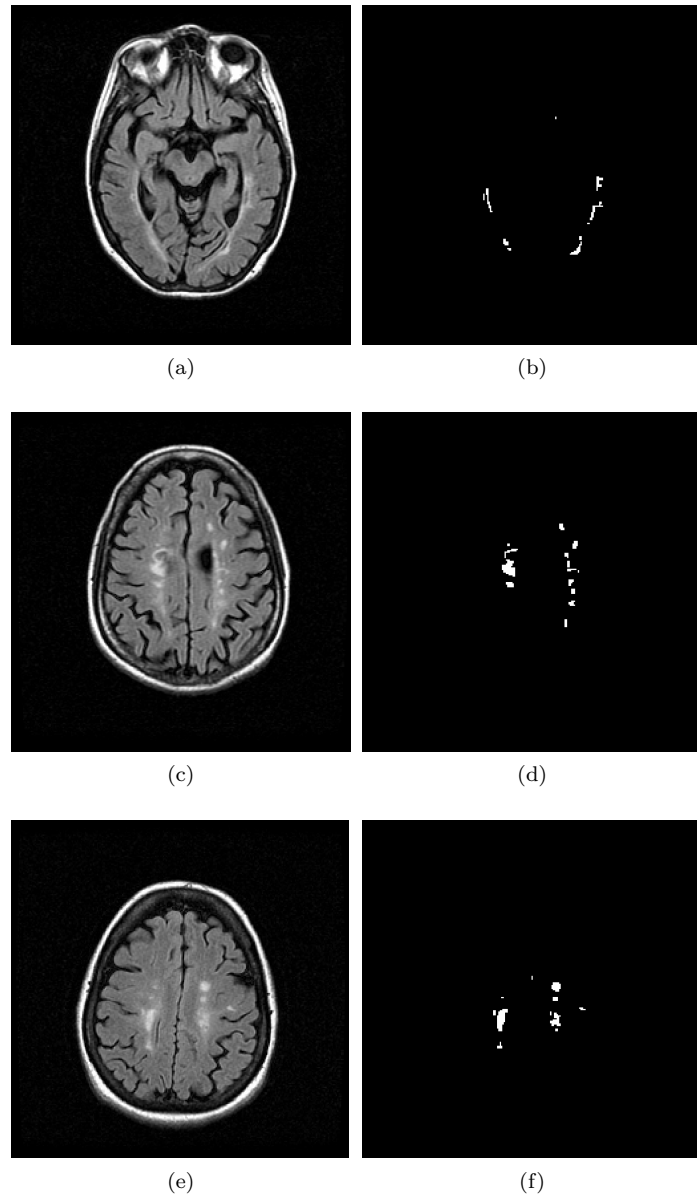
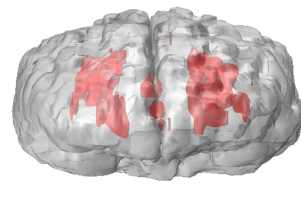
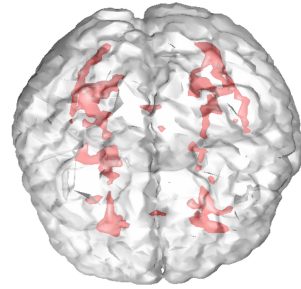


Fig. 14: Segmentation of MRI for MS lesions detection by using CNN.

Simulations (Figure 14) have allowed to verify the validity of the proposed algorithm; the output generated by CNN can be viewed in MRICro medical image viewer (<http://www.mricro.com>). Once the number of pixels corresponding to the injury has been determined and knowing the size of the voxel in the performed scan, it is possible to estimate the total lesion load for a given patient, that provides an important parameter to monitor the progression of the disease. It should be emphasized that the results in Figure 14 were obtained without operating any manual thresholding operation; in other words, the proposed algorithm allows to fully automate the process of estimating lesion load for a given patient. Obviously, operating a manual tuning of the network, the algorithm is able to produce more accurate results. Overlapping the slices and the output of CNN, is possible to obtain a 3D reconstruction of the brain of the patient, which displays an estimate of brain tissue sclerosis (Figure 15).



(a)



(b)

Fig. 15: Three-dimensional reconstruction of the lesions detected by using CNN.

Sometimes, the images acquired by MRI systems have, from patient to patient, significant differences in the intensity of grey and injuries, as indeed it has been observed also from a slice to another; for this reason, it is necessary to train the network adapting it to conditions not encountered before. However, the results obtained by applying the proposed algorithm have been very convincing, since CNN can determine most of the lesions and thus it could provide a useful support tool for the diagnosis of pathology in particular to assess the presence and the evolution of the lesions. Efforts are under way for improving templates obtained by GA. Some snapshots of the software we have implemented are shown in Figure 16.

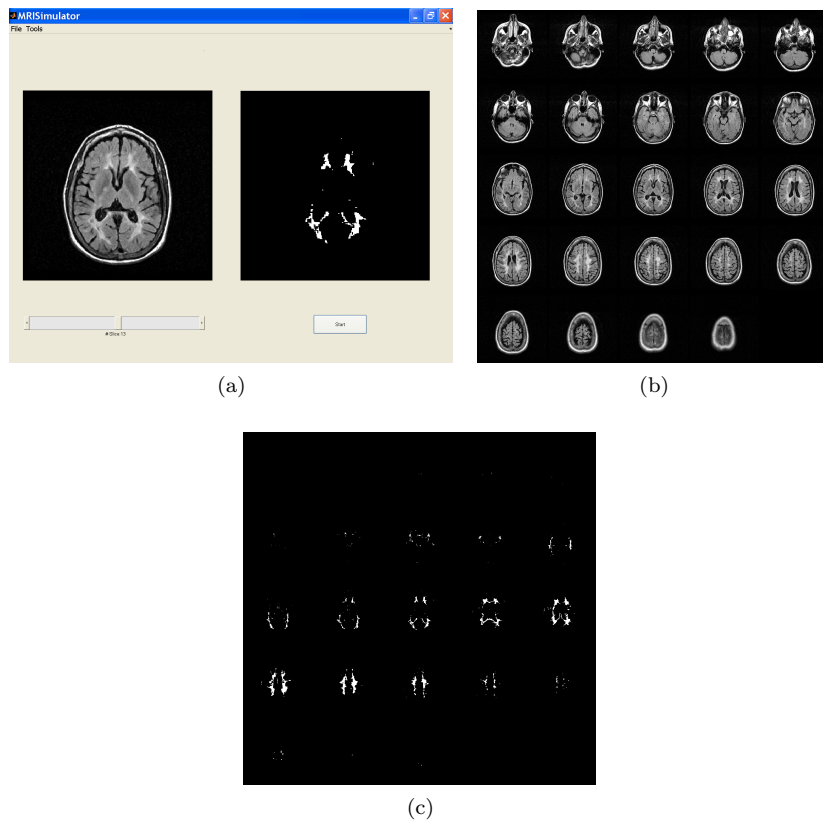


Fig. 16: Snapshots of the software we have developed. (a) Main window of the software (b) Input of the simulation (c) Output of the simulation.

The experiments presented above have been carried out by using an algorithm based on two-dimensional data. The new idea is to extend our results by working on volumes of data, rather than processing planar images. 3D CNNs may represent a new and powerful tool for the development of appli-

cations for supporting medical diagnosis; in fact, by exploiting information provided by a three dimensional representation of the brain, the evolution of the 3D network can lead to a significant improvement of the performances. For this reason, by modifying the architecture of the standard CNN, we propose a 3D CNN model that is able to handle and perform different functions on objects in a three dimensional space. We consider an array of $M \times N \times P$ dynamical systems; in this case, each cell is referenced by the triple (i, j, k) , and the evolution of the state is described by the following set of ODEs:

$$\begin{aligned} \frac{dx_{ijk}(t)}{dt} = & -x_{ijk}(t) + \\ & \sum_{C(l,m,n) \in S_r(i,j,k)} A(i, j, k; l, m, n) y_{lmn}(t) + \\ & \sum_{C(l,m,n) \in S_r(i,j,k)} B(i, j, k; l, m, n) u_{lmn} + z_{ijk} \\ y_{ijk}(t) = f(x_{ijk}(t)) = & \frac{1}{2} [|x_{ijk}(t) + 1|] - [|x_{ijk}(t) - 1|] \end{aligned} \quad (14)$$

where A and B contain the synaptic weights between C_{ijk} and its neighbours, and z_{ijk} denotes the bias of the cell. We define the sphere of influence of radius r of C_{ijk} , denoted by $S_{ijk}(r)$, as the set of cells satisfying the following property:

$$S_{ijk}(r) = \{C(l, m, n) \mid \max_{1 \leq l \leq M, 1 \leq m \leq N, 1 \leq n \leq P} \{|l - i|, |m - j|, |n - k|\} \leq r\}, \quad r \geq 0 \quad (15)$$

This means that, assuming $r = 1$, a $3 \times 3 \times 3$ neighbourhood is associated to each cell, i.e. each processing unit has 27 neighbors (including the cell itself). Figure 17 shows the $3 \times 3 \times 3$ neighbourhood for the cell at the position (i, j, k) (reported as grey); to avoid cluttering, only connections between C_{ijk} and its neighbors are shown.

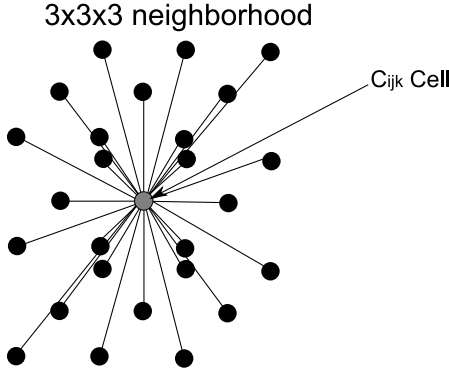


Fig. 17: Neighbourhood for the cell C_{ijk} of a 3D-CNN.

Therefore, for a space-invariant 3D-CNN, the feedback operator is given by the array $A \in \mathbb{R}^{3 \times 3 \times 3}$, the control operator is $B \in \mathbb{R}^{3 \times 3 \times 3}$ and so 55 parameters are needed in order to define a template $\{A, B, z\}$ for a 3D-CNN. An innovative library of 3D templates has been implemented, that allows to execute interesting and efficient operations, as shown in Figures 18 and 19.

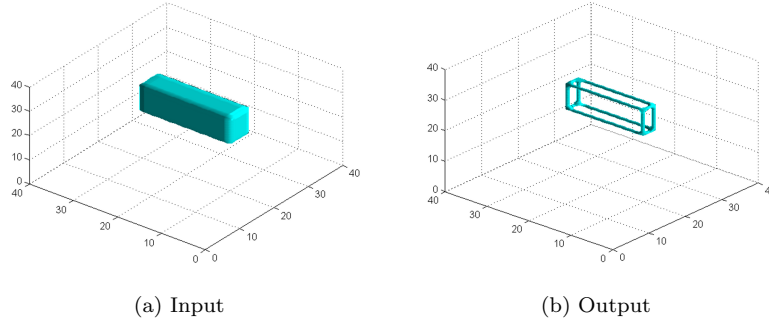


Fig. 18: Edge corners detection.

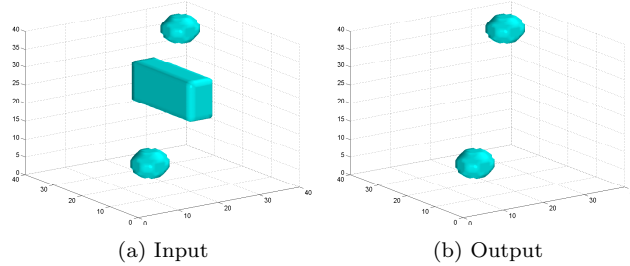


Fig. 19: Spherical objects detection.

We used genetic algorithms for 3D template learning; this means that even a 3D-CNN can be trained by a learning algorithm in such a way that, during the training process, the network learns which is the configuration for performing the desired operation. The slices acquired from a MRI scanning can be recasted into a three dimensional array and provided as input to the 3D-CNN; a 3D visualization of the input, obtained by superimposing 24 slices for a given patient, is shown in Figure 20. In this way, the analysis of MRI images can be performed according to the cellular neural network model (14). The template used for the segmentation of MS lesions on planar images (13) has been adapted in order to construct a $3 \times 3 \times 3$ template to be used for 3D-CNNs.

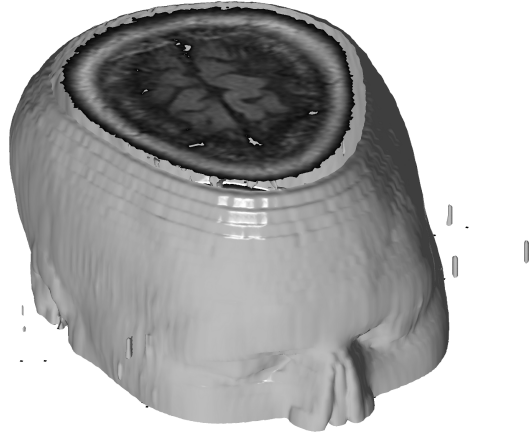


Fig. 20: 3D visualization of MRI slices re-casted into an array $256 \times 256 \times 24$.

Again, after detecting lesions inside the brain area (Figure 21(a)), by applying 3D templates we've found for operations on volumetric data, “noise removal” is performed and voxels corresponding to MS lesions are segmented, as shown in Figure 21(b).

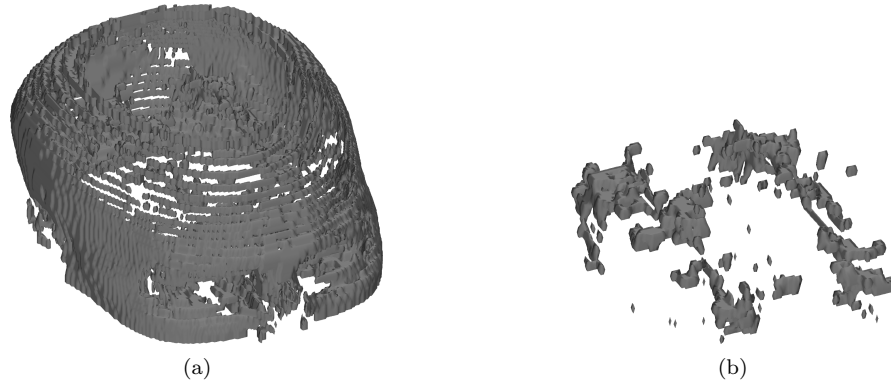


Fig. 21: CNN processing of MRI volumetric data. A 3D surface representation of sub-cortical structure and lesions, generated from the results of our method. Note how the 3D rendering outlines the global structure of the lesions.

4.3 Integration into the Productive System and with other software or hardware components

We are integrating this system within the Institute of Neurological Sciences, National Research Council, Piano Lago di Mangone, Cosenza, in collaboration with the Faculty of Medicine, University “Magna Græcia” of Catanzaro. Meanwhile we are expanding the number of patients to least 10 for each step of the EDSS scale, for a total of 100 patients. We are trying to correlate TLLs, found via the automated approach that we have developed, with clinical signs of MS, in correlation with the EDSS. We are also conducting a study on the evolution of the disease, in correlation with the increase of lesion load. We are trying to find “the clinical impossible”, i.e. intermediate lesion load observed in the scale of functional systems, that cannot be assessed by neurologists. Instead, by using the CNN automated segmentation method, we could research interstitial values of lesion load related to different disabilities in both cognitive and motor skills. These results could be very useful in the management of MS patients therapies, thus allowing this method to work in a real life situation. Moreover, given the possibility of implementing in hardware the CNNs based algorithm, we could even integrate the chip as a system embedded in the MRI machine, as an extension of the system. This method can also be generalized to other diseases and other forms of brain imaging technologies. Furthermore, the method has practical application as it can be used both for diagnostic purposes and for training medical professionals.

5 Experimental Results

The experiment described in this section compares the accuracy of the CNN based segmentation method, we have presented in the previous sections, with manual delineations of multiple sclerosis lesions. The second approach is similar to the CNN based approach but it consists of different non automatic steps. Both methods utilize the same set of data, which captures the spatial distributions of the TLL in brain white matter. The training data of the experiment consists for both methods of sequence of magnetic resonance images, as the examples in Figures 13. The data are generated through the approach suggested by Warfield et al. [73], which aligns the training subjects to a pre-selected training case and then measures the overlap between the corresponding segmentations. Each method segments the same number of cases. Magnetic resonance imaging scanning was performed on a 1.5 T Unit (Signa NV/i, General Electric, Milwaukee, Wisconsin) using a standard quadrature head coil. 2D fast fluid-attenuated inversion-recovery (FLAIR) axial images (TR 8000ms, TE 120ms; 256 × 224 image matrix, FOV: 24cm; 24 slices, 4mm slices, 1 – mm gap) oriented along the AC-PC line were used

to calculate hyper-intense lesion load. We have evaluated the accuracy of the approaches by measuring the agreement of the automatic segmentations of the TLL to the manual ones. Note that the other method greatly depends on the precise segmentation of white matter as the MS disease is characterized of weakly visible boundary. The performances of the process have been quantitatively evaluated by comparing the CNN output and the expert's manual delineation of MS lesions, using the Dice coefficient [74] as a metric. The Dice coefficient D is a statistic measure used for comparing the extent of spatial overlap between two binary images. It is commonly used in reporting performance of segmentation and its values range between 0 (no overlap) and 1 (perfect agreement). In this work, the Dice values, expressed as percentages, are computed as follows:

$$D = \frac{2|L^{CNN} \cap L^G|}{|L^{CNN}| + |L^G|} \times 100 \quad (16)$$

where L^{CNN} is the automated segmentation result and L^G the manual one. The graph in Figure 22 shows the Dice measure for the three compared templates in the 11 cases.

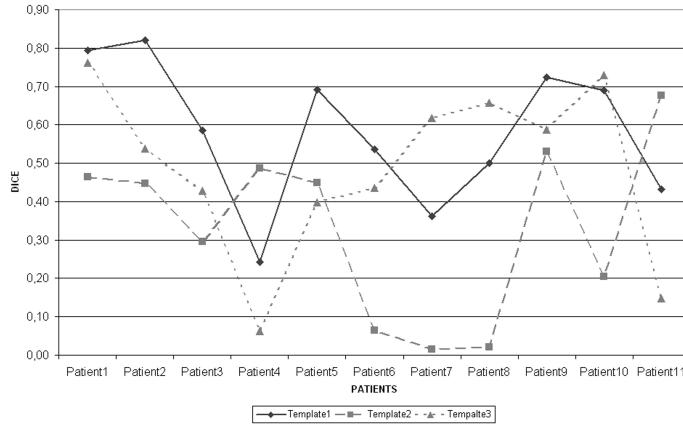


Fig. 22: Dice measures for Template1, Template2, Template3.

We have compared quantitatively the performance of the three templates compared to the gold standard represented by the manual measures. The results can be summarized as follows:

1. The template appears to be the best Template1, with an average overlap ratio 0.58 compared to the gold standard handbook (1 perfect overlap, 0 no overlap); Template1 is absolutely the best 6/11 = 55% subjects, respec-

- tively, followed by Template3 in $3/11 = 27\%$ of subjects and Template2 in $2/11 = 18\%$.
2. The template is what Template2 are more likely to under-segmented.
 3. The template is what Template3 are more likely to over-segmented.

Proportionally, the average error of under-segmentation of Template2 (1.25) is greater than that of over-segmentation of Template3 (0.89). From Figure 22 is possible to observe that, by applying Template1, the highest Dice measure is achieved for Patient2 (~ 0.82), while the algorithm produces the lowest value (~ 0.24) on Patient4. The method we have implemented for automatically segmenting MS lesions gives satisfactory results, showing that after the learning process the CNN is capable of detecting MS lesions with different shapes and intensities, even in MRI slices with different contrasts between white and grey matter, with respect to the images used during the genetic training process. Thus, the proposed algorithm provides a good robustness. It is worth noting that training images, as well as the ones used for testing, come from a data set of real MS patients and MRI are not pre-processed. The algorithm is run directly on the slices as they are acquired by the magnetic resonance. The aim is to provide a tool that does not require any manual operation for the physicians, and the training process is still underway in order to improve the robustness furthermore. The vast majority of the lesion load, detected by CNN for the described sample, ranges from $D = 0.6$ to $D = 0.8$. The technique we propose for segmenting white matter lesions in MS is a fully automatic method and does not require manually segmented data; in fact, while semiautomatic methods are highly dependent on the choice of an appropriate threshold to effectively detect lesions (threshold that usually may vary between different slices even for the same patient, thus leading to a time consuming task), our algorithm allows for obtaining the desired output by programming a fully automated strategy on the entire data set, without the need of external calibration. Simulations have allowed to verify the validity of the above described algorithm. The output generated by the CNN can also be viewed in MRIcro medical image viewer. Calculating the number of pixels corresponding to the injury and knowing the size of the voxel used in the scanning, it is possible to estimate the TLL for any patient. This method provides an important parameter to monitor the progress of the pathological disease. It should be emphasized that the results were obtained without changing the template from one slice to another.

6 Conclusions

In this paper, we presented a new completely automatic segmentation technique for detecting MS lesions in white matter regions of the brain. The performance of the method has been evaluated compared to manual segmentation. The results, obtained by applying the proposed algorithm, are very

convincing, since the CNN system can determine most of the lesions in all the patients. The method we have implemented could provide a useful MR support tool for the evaluation of lesions in MS, particularly to assess the evolution of the lesions. From a comparison with other existing methods in the literature on this topic, we can say that the results are valuable and the threshold of recognition is currently at 70%. Furthermore, it should be emphasized the real improvement of the proposed method with respect to our previous work due the greater accuracy of the system, its adaptation to different conditions of the stimuli, its ability to create 3D images of the injured areas of the brain, thus effectively supporting medical diagnosis. With this method, slighter changes in the total lesion load can be detected, improving both our knowledge of the disease and our ability to monitor it.

7 Future Work

MS lesions have a complex evolution that begins with an initial disruption of blood brain barrier, accompanied by demyelination, inflammation, axonal damages. Later on the disease appears to regress partially. So far clinical studies and the characteristics of the MRI technology have allowed the identification of the evolution of this disease, although three main groups of lesions have identified. This classification includes:

- a Acute lesions demonstrated by losses in the blood-brain barrier, detected in contrast-MR Advanced imaging (enhancing lesions);
- b Chronic wounds severely damaged, hypointense so-called “black holes”, visible n T1-weighted MR images (T1WI);
- c Hyperintense lesions, detectable in T2 (T2 lesions), visible on T2-weighted MRI (T2WI).

This classification of MS lesions in these subtypes is widely accepted and has demonstrated good clinical utility in the related studies [75, 76]. Future work foresees to automatically segment, with the CNNs based method, MS lesions into the above mentioned three subtypes, in different brain tissue compartments. To do this, we shall use different sequences of magnetic resonance images, that identify different stages of evolution of the disease. We also want to divide MRI by using a grid, like a chessboard, in order to locate in which quadrant of the grid the lesions settled. This would enable us to correlate the location of the lesions in the brain with a more accurate identification of the specific disabilities of each patient. We also want to see if it is possible to study the patterns of this disease through the application of methods of chaos and nonlinear dynamical systems, intercepting sensitivity to initial data, variables for each subject, the possibility of developing the disease within a parameter space, the evolution of the patterns of MS injuries.

References

1. L. Lanzarini and A. De Giusti. Pattern recognition in medical images using neural networks. *Journal of Computer Science and Technology*, 2001.
2. A. Wismuller, F. Vietze, and Dersch D.R. Segmentation with Neural Networks. In *Handbook of Medical Image Processing and Analysis*, chapter 7, pages 113–143. Elsevier, Johns Hopkins University, Baltimore, MD, USA, 2008.
3. J.S. Suri, D.L. Wilson, and S. Laxminarayan. Segmentation Models, Part B. In *Handbook of Biomedical Image Analysis*, volume 2, chapter 7, pages 315–368. Kluwer Academic/Plenum Publishers, New York, 2005.
4. A. Wismuller, A. Meyer-Bease, O. Lange, D. Auer, M.F. Reiser, and D. Sumners. Model-free functional MRI analysis based on unsupervised clustering. *Journal of Biomedical Informatics*, (37):10–18, 2004.
5. G.L. Leinsinger, A. Wismuller, P. Joechel, O. Lange, D.T. Heiss, and K. Hahn. Evaluation of the motor cortex using fMRI and image processing with self-organized cluster analysis by deterministic annealing. *Radiology*, pages 221–487, 2001.
6. A. Wismuller, D.R. Dersch, B. Lipinski, K. Hahn, and D. Auer. Hierarchical Clustering of Functional MRI Time-Series by Deterministic Annealing . In *Lecture Notes in Computer Science*, volume 1933/2000, pages 83–118. Springer, Berlin/Heidelberg, 2000.
7. F. Döhler, F. Mormann, B. Weber, C.E. Elger, and K. Lehnertz. A cellular neural network based method for classification of magnetic resonance images: Towards an automated detection of hippocampal sclerosis. *Journal of neuroscience methods*, 170(2):324–331, 2008.
8. L.O. Chua and L. Yang. Cellular Neural Networks: Theory. *IEEE Transaction on Circuits and Systems*, 35(10):1257–1272, 1988.
9. L.O. Chua. *CNN: A paradigm for Complexity*. World Scientific Series on Nonlinear Science, 1996.
10. L.O. Chua and T. Roska. Cellular Neural Networks and Visual Computing: Foundations and Applications. *Cambridge University Press*, 2004.
11. C. Niederhoefer, F. Gollas, and R. Tetzlaff. EEG analysis by multi layer Cellular Nonlinear Networks (CNN). *Biomedical Circuits and Systems Conference, IEEE*, 2006.
12. T. Schwarz, T. Heimann, R. Tetzlaf, A.M. Rau, I. Wolf, and H.P. Meinzer. Interactive Surface Correction for 3D Shape Based Segmentation. *Medical Imaging*, 2008.
13. E. Bilotta, A. Cerasa, P. Pantano, A. Quattrone, A. Staino, and F. Stramandinoli. A CNN Based Algorithm for the Automated Segmentation of Multiple Sclerosis Lesions. 2010. EvoStar 2010 Conference, ITU, Istanbul, Turkey, (In press).
14. L.O. Chua. *A Nonlinear Dynamics Perspective of Wolfram’s New Kind of Science*. World Scientific Publishing Co. Singapore, 2007.
15. T. Roska, L.O. Chua, D. Wolf, T. Kozek, and R. Tetzlaff. Simulating Nonlinear Waves and Partial Differential Equations via CNN. *IEEE Transaction on Circuits and Systems*, 42(10), 1995. Part I: Basic Techniques.
16. T. Kozek, L.O. Chua, T. Roska, D. Wolf, R. Tetzlaff, F. Pufferand, and K. Lotz. Simulating Nonlinear Waves and Partial Differential Equations via CNN. *IEEE Transaction on Circuits and Systems*, 42(10), 1995. Part 11.
17. P. Arena, A. Basile, M. Bucolo, and L. Fortuna. Image processing for medical diagnosis using CNN. In *Nuclear Instruments and Methods A*.
18. T. Szabo, P. Barsi, and P. Szolgay. Application of Analogic CNN algorithms in Telemedical Neuroradiology. *Journal of Neuroscience Methods*, 170(7):2063–2090, 2005.
19. L. Kek, K. Karacs, and T. Roska. *Cellular Wave Computing Library (Templates, Algorithms and Programs ver.2.1)*, 2007. Cellular Sensory Wave Computers Laboratory, Hungarian Academy of Science.

20. B.D. Trapp, R. Ransohoff, and R. Rudich. Axonal pathology in multiple sclerosis: relationship to neurologic disability. In *Current Opinion in Neurology*.
21. B.M. Keegan and J.H. Noseworthy. Multiple sclerosis. *Annual Review of Medicine*, (53):285–302, 2002.
22. H. Lassmann. Cellular damage and repair in multiple sclerosis. In *Myelin Biology and Disorders*, pages 753–762. Lazzarini, R.A. (Ed.) Elsevier, 2004.
23. A. Ozturk, S. Smith, E. Gordon-Lipkin, D. Harrison, N. Shiee, D. Pham, B. Caffo, P. Calabresi, and D. Reich. Mri of the corpus callosum in multiple sclerosis: association with disability. *Multiple sclerosis*, 16(2):166–77, 2010.
24. J. F. Kurtzke. Rating neurologic impairment in multiple sclerosis: an expanded disability status scale (edss). *Neurology*, 33(11):1444–1452, November 1983.
25. D. M. Gronwall. Paced auditory serial-addition task: a measure of recovery from concussion. *Percept Mot Skills*, (44):367–373, 1977.
26. K. Young and N. Schuff. Measuring Structural Complexity in Brain Images. *NeuroImage*, 39(4):1721–1730, 2008.
27. A. Giorgio, J. Palace, H. Johansen-Berg, S.M. Smith, Fuchs S. Ropele, S., M. Wallner-Blazek, C. Enzinger, and F. Fazekas. Relationships of brain white matter microstructure with clinical and MR measures in relapsing-remitting multiple sclerosis. *Journal of magnetic resonance imaging*, 31(2):309–16, 2008.
28. J.S. Wonderlick, D.A. Ziegler, P. Hosseini-Varnamkhasti, J.J. Locascio, A. Bakkour, A. Van Der Kouwe, C. Triantafyllou, S. Corkin, and B.C. Dickerson. Reliability of mri-derived cortical and subcortical morphometric measures: effects of pulse sequence, voxel geometry, and parallel imaging. *Neuroimage*, 44(4):1324–1333, 2009.
29. Y. Wu, S.K. Warfield, I. Tan, W.M. Wells, D.S. Meier, R. Van Schijndel, F. Barkhof, and C.R. Guttman. Automated segmentation of multiple sclerosis lesion subtypes with multichannel mri. *NeuroImage*, 32(3):1205–1215, 2006.
30. A. Akselrod-Ballin, M. Galun, J.M. Gomori, M. Filippi, P. Valsasina, R. Basri, and A. Brandt. Automatic segmentation and classification of multiple sclerosis in multi-channel mri. *IEEE Transactions on Biomedical Engineering*, 56(10), 2009.
31. V. Zharkova and L. Jain. Introduction to pattern recognition and classification in medical and astrophysical images. In *Artificial Intelligence in Recognition and Classification of Astrophysical and Medical Images*, volume 46 of *Studies in Computational Intelligence*, pages 1–18. Springer Berlin / Heidelberg, 2007.
32. D. Brzakovic, X.M. Luo, and P. Brzakovic. An Approach to Automated Detection of Tumors in Mammograms. *IEEE Transactions on Medical Imaging*, 9(3), 1990.
33. G. Ertas, H.O. Gulcur, O. Osman, O.N. Ucan, M. Tunaci, and M. Durusun. Breast MR segmentation and lesion detection with cellular neural networks and 3D template matching. *Computers in Biology and Medicine*, (38):116–126, 2008.
34. M.H. Brem, P.K. Lang, G. Neumann, P.M. Schlechtweg, E. Schneider, R. Jackson, J. Yu, C.B. Eaton, F.F. Hennig, H. Yoshioka, G. Pappas, and J. Duryea. Magnetic resonance image segmentation using semi-automated software for quantification of knee articular cartilage-initial evaluation of a technique for paired scans. *Radiology*, (38):505–511, 2009.
35. M. Filippi, T. Yousry, C. Baratti, M.A. Horsfield, S. Mammi, C. Becker, R. Voltz, S. Spuler, A. Campi, M.F. Reiser, and G. Comi. Quantitative assessment of MRI lesion load in multiple sclerosis. *Brain*, (119):1349–1355, 1996.
36. J.C. Souplet, C. Lebrun, S. Chanalet, N. Ayache, and G. Malandain. Approaches to segment multiple-sclerosis lesions on conventional brain MRI. *Rev Neurol*, 165(1):7–14, 2009.
37. N. Shiee, P.L. Bazin, A. Ozturk, D.S. Reich, P.A. Calabresi, and D.L. Pham. A topology-preserving approach to the segmentation of brain images with multiple sclerosis lesions. *Neuroimage*, 2009. in press.
38. H. Larochelle, Y. Bengio, J. Louradour, and P. Lamblin. Exploring Strategies for Training Deep Neural Networks. *Journal of Machine Learning Research*, 10:1–40, 2009.

39. C. M. Bishop. *Pattern Recognition and Machine Learning*. Springer-Verlag, 2006.
40. E. Bilotta and P. Pantano. Cellular Non-Linear Networks as a New Paradigm for Evolutionary Robotics. In *Frontiers in Evolutionary Robotics*, pages 87–108. Hitoshi Iba, Vienna, Austria.,
41. E. Bilotta, P. Pantano, and F. Stranges. A Gallery of Chua Attractors. *Int. J. of Bifurcation and Chaos*, 17(1):1–60, 2007. Part I.
42. E. Bilotta, P. Pantano, and F. Stranges. A Gallery of Chua Attractors. *Int. J. of Bifurcation and Chaos*, 17(2):293–380, 2007. Part II.
43. E. Bilotta, P. Pantano, and F. Stranges. A Gallery of Chua Attractors. *Int. J. of Bifurcation and Chaos*, 17(3):657–734, 2007. Part III.
44. E. Bilotta, P. Pantano, and F. Stranges. A Gallery of Chua Attractors. *Int. J. of Bifurcation and Chaos*, 17(4):1017–1078, 2007. Part IV.
45. E. Bilotta, P. Pantano, and F. Stranges. A Gallery of Chua Attractors. *Int. J. of Bifurcation and Chaos*, 17(5):1383–1511, 2007. Part V.
46. E. Bilotta, P. Pantano, and F. Stranges. A Gallery of Chua Attractors. *Int. J. of Bifurcation and Chaos*, 17(6):1801–1910, 2007. Part VI.
47. A.E. MacDonald, J.L. Lee, and S. Sun. QNH: Design and test of a quasi-nonhydrostatic model for mesoscale weather prediction. *M. Weather Rev.*, (128):1016–1036, 2000.
48. A.J. Anand, D.W. Shattuck, D. Pantazis, Q. Li, H. Damasio, and R.M. Leahy. Optimization of landmark selection for cortical surface registration. *CVPR 2009*, pages 699–706, 2009.
49. A.J. Anand, R.M. Leahy, A.W. Toga, and D.W. Shattuck. A Framework for Brain Registration via Simultaneous Surface and Volume Flow. *IPMI 2009*, pages 576–588, 2009.
50. P. Schneider, M. Andermann, M. Wengenroth, R. Goebel, H. Flor, A. Rupp, and E. Diesch. Reduced volume of Heschl’s gyrus in tinnitus. 2009.
51. J. Ylipaavalniemi and R. Vigario. Analyzing consistency of independent components: an fMRI illustration. *Neuroimage*, 1;39(1):169–80, 2008.
52. J.P. Wachs, H.I. Stern, Y. Edan, M. Gillan, J. Handler, C. Feied, and M. Smith. A gesture-based tool for sterile browsing of radiology images. *Journal of the American Medical Informatics Association*, 15(3):321–324, 2008.
53. P.M. Thompson, C. Vidal, J.N. Giedd, P. Gochman, J. Blumenthal, R. Nicolson, A.W. Toga, and J.L. Rapoport. Mapping adolescent brain change reveals dynamic wave of accelerated gray matter loss in very early-onset schizophrenia. *The Journal of Neuroscience*, 21(22):8819–8829, 2001.
54. Y. Wang, J. Zhang, B. Gutman, T.F. Chan, J.T. Becker, H.J. Aizenstein, O.L. Lopez, R.J. Tamburo, A.W. Toga, and P.M. Thompson. Multivariate tensor-based morphometry on surfaces: application to mapping ventricular abnormalities in HIV/AIDS. *Neuroimage*, 1;49(3):2141–2157, 2010.
55. D. Tosun and J.L. Prince. A geometry-driven optical flow warping for spatial normalization of cortical surfaces. *IEEE Transaction of Medical Imaging*, 27(12):1739–1753, 2008.
56. A.C. Vernon, S.M. Johansson, and M.M. Modo. Non-invasive evaluation of nigrostriatal neuropathology in a proteasome inhibitor rodent model of Parkinson’s disease. *BMC Neurosci.*, 11(1), 2010.
57. A. Labate, A. Gambardella, U. Aguglia, F. Condino, P. Ventura, and P. Lanza. Temporal lobe abnormalities on brain MRI in healthy volunteers: A prospective case-control study. *A. Neurology*, 16;74(7):553–557, 2010.
58. K.V. Leemput, F. Maes, D. Vandermeulen, A. Colchester, and P. Suetens. Automated segmentation of multiple sclerosis lesions by model outlier detection. *IEEE Transactions on Medical Imaging*, 20(8):677–688, 2001.
59. O. Freifeld, H. Greenspan, and J. Goldberger, editors. *Lesion detection in noisy MR brain images using constrained GMM and active contours (ISBI 2007)*. 4th IEEE International Symposium on Biomedical Imaging, 2007.

60. L.S. Aït-Ali, S. Prima, P. Hellier, B. Carsin, G. Edan, and C. Barillot. STREM: A Robust Multidimensional Parametric Method to Segment MS Lesions in MRI. In James S. Duncan and Guido Gerig, editors, *Medical Image Computing and Computer-Assisted Intervention - MICCAI 2005*, volume 3749 of *Lecture Notes in Computer Science*, pages 409–416. Springer Berlin / Heidelberg, 2005.
61. S. Bricq, C. Collet, and J.P. Armanpach, editors. *Lesion detection in 3D brain MRI using trimmed likelihood estimator and probabilistic atlas (ISBI 2008)*. 5th IEEE International Symposium on Biomedical Imaging, 2008.
62. D. Garcia-Lorenzo, S. Prima, D. Collins, D. Arnold, S. Morrissey, and C. Barillot, editors. *Combining robust expectation maximization and mean shift algorithms for multiple sclerosis brain segmentation (MIAMS08)*. MCRAI workshop on Medical Image Analysis on Multiple Sclerosis, 2008.
63. R. Harmouche, L. Collins, D. Arnold, S. Francis, and T. Arbel, editors. *Bayesian MS lesion classification modeling regional and local spatial information (ICPR 2006)*. 18th International Conference on Pattern Recognition, 2006.
64. D.P. Ramasamy, R. Benedict, J.L. Cox, D. Fritz, N. Abdelrahman, S. Hussein, A. Minagar, M.G. Dwyer, and R. Zivadinov. Extent of cerebellum, subcortical and cortical atrophy in patients with ms: a case-control study. *Journal of the Neurological Sciences*, 282(1-2):47–54, 2001.
65. F. Beltrame and S.H. Koslow. Neuroinformatics as a megascience issue. *IEEE Trans. Inf. Technol. Biomed.*, 3:339–340, 1999.
66. M. Bota and M.A. Arbib. The NeuroHomology Database. In *Computing the brain: A guide to neuroinformatics*, pages 337–351. M. A. Arbib, and J. Grethe (Eds.), New York: Academic Press, 2001.
67. G.A.P.C. Burns, K.E. Stephan, B. Lüdässcher, A. Gupta, and R. Kötter. Towards a federated neuroscientific knowledge management system using brain atlases. *Neurocomputing*, 38(40):1633–1641, 2001.
68. D.W. Shattuck and R.M. Leahy. Graph Based Analysis and Correction of Cortical Volume Topology. *IEEE Transactions on Medical Imaging*, 20(11):1167–1177, 2001.
69. V. Megalooikonomou, J. Ford, L. Shen, F. Makedon, and F. Saykin. Data mining in brain imaging. *Statistical Methods in Medical Research*, 9:359–394, 2000.
70. J.C. Mazziotta, A.W. Toga, A.C. Evans, P. Fox, and J. Lancaster. A probabilistic atlas of the human brain: theory and rationale for its development. *NeuroImage*, 2(2):89–101, 1995.
71. R. Caponetto, L. Fortuna, and M. Frasca. *Advanced Topics on Cellular Self-Organizing Nets and Chaotic Nonlinear Dynamics to Model and Control Complex Systems*, volume 63. World Scientific Series on Nonlinear Science.
72. J. Holland. *Adaptation in natural and artificial systems*. University of Michigan Press, 1975.
73. S.K. Warfield, J. Rexilius, P.S. Huppi, T.E. Inder, E.G. Miller, W.M. Wells, III, G.P. Zientara, F.A. Jolesz, and R. Kikinis. A binary entropy measure to assess nonrigid registration algorithms. In *in MICCAI*, pages 266–274. Springer, 2001.
74. L. R. Dice. Measures of the amount of ecologic association between species. *Ecology*, 26(3):pp. 297–302, 1945.
75. F. Barkhof, J.H. Van Waesberghe, and M. Filippi. T(1) hypointense lesions in secondary progressive multiple sclerosis: effect of interferon beta-1b treatment. *Brain*, (124):1396–1402, 2001.
76. D.W. Paty and D.K. Li. Interferon beta-1b is effective in relapsing remitting multiple sclerosis: II. MRI analysis results of a multicenter, randomized, double-blind, placebo-controlled trial. *Neurology*, (57), 1993.